Cone Penetration Testing 2022 – Gottardi & Tonni (eds)

Characterisation of near-surface sediments using a blend of vertical and shallow rotational penetrometers

D.J. White
University of Southampton, UK

S.A. Stanier
University of Cambridge, UK

H. Mohr
University of Western Australia and MSMT Solutions, Perth, Australia

ABSTRACT: The mechanical properties of near-surface sediments – to a depth of approximately half a metre – are relevant to the design of cables, pipelines and other shallowly-embedded infrastructure, as well as benthic habitat characterisation. For this depth of interest, vertically-pushed penetrometers – such as the cone, T-bar or ball – can be supplemented by shallow rotational devices such as the toroid or hemiball. In this paper, we report vertical and shallow rotational penetrometer test procedures and show results obtained in project conditions on natural soil samples. By combining these different penetrometers, a wider and more reliable set of mechanical properties – spanning strength and consolidation behaviour – can be obtained, compared to conventional practice. The paper concludes with practical advice on testing protocols and interpretation methods to best characterise the shallow seafloor, including the use of novel shallow penetrometers.

1 INTRODUCTION

1.1 *Shallow seabed properties*

The properties of the shallowest half metre of the seabed are relevant to the design of cables, pipelines and other shallowly-embedded infrastructure such as rock dump and scour protection systems, as well as the study of benthic ecosystems. The importance of accurately determining the strength and consolidation properties of the seafloor is emphasized in good practice guidance (e.g. ISO 19901-4, White et al. 2017).

Typical practice to characterize the shallowest seafloor includes (i) box core or drop core sampling, (ii) penetrometer testing from a seabed frame or into a box core and (iii) index testing of samples.

In this paper, we describe how practice can be enhanced by modern vertical and shallow rotational penetrometer testing to determine more accurately the strength and consolidation properties of the seafloor.

1.2 *Novel shallow penetrometer systems*

Shallow penetrometers, which combine vertical movement and rotation about the vertical axis, were first trialled a decade ago, using toroid and hemiball shapes (Yan et al. 2010). Subsequent work includes laboratory studies (e.g. Boscardin & de Groot 2015, Schneider et al. 2020a) and numerical simulations (Stanier & White 2015, Yan et al. 2017, Schneider et al. 2020b,c). Some of this work formed part of the Remote Intelligent Seabed Surveys (RIGSS) Joint Industry Project (www.rigssjip.com).

2 COMBINED PENETROMETER SYSTEM

2.1 *Actuation system*

A shallow penetrometer test aims to subject the seabed to a loading history that replicates the conditions around infrastructure, and provides a simple basis to interpret fundamental soil properties, including the interface shear strength at the penetrometer surface. The control requirements involve vertical and rotational motion in load-controlled contact with the seabed. These requirements exceed current systems for CPT and T-bar testing, which involve only vertical motion between specified position limits.

A system for vertical and shallow penetrometry must therefore meet the following requirements:

1. Accurate identification of the touchdown point, when the penetrometer contacts the seabed.
2. Control via feedback of the vertical load on the penetrometer, e.g. during a dissipation step.

DOI: 10.1201/9781003308829-33

3. Allow 'programmable motion control' so that sequences (e.g. penetration-dissipation-rotation) can be performed without intervention.
4. Allow variable speeds of movement to permit testing over a range of drainage conditions.

An actuator system that meets these requirements was developed as part of the RIGSS Joint Industry Project (Figure 1, Schneider et al. 2020a). The capabilities are summarised as follows:

1. Controlled motion at rates of 0-3 mm/s (vertical) and 0-3 deg/s (rotational), allowing drained and undrained movements in clay and silt soils (drained in sand), with positioning resolution of 0.0125 μm and 9×10^{-6} degrees.
2. Load measurement and control to an accuracy of ± 0.1 N, even on-deck under ship motion – as proven during offshore trials. This force resolution corresponds to less than 0.02 kPa of undrained strength, for the sizes of shallow penetrometer used, so the system accuracy is much better than typical sample variability.
3. A user interface and motion control system allows pre-programmed steps of consolidation (under set vertical load) and/or cyclic rotation.
4. Ruggedised packaging in plastic flight cases allows transport offshore or by plane.

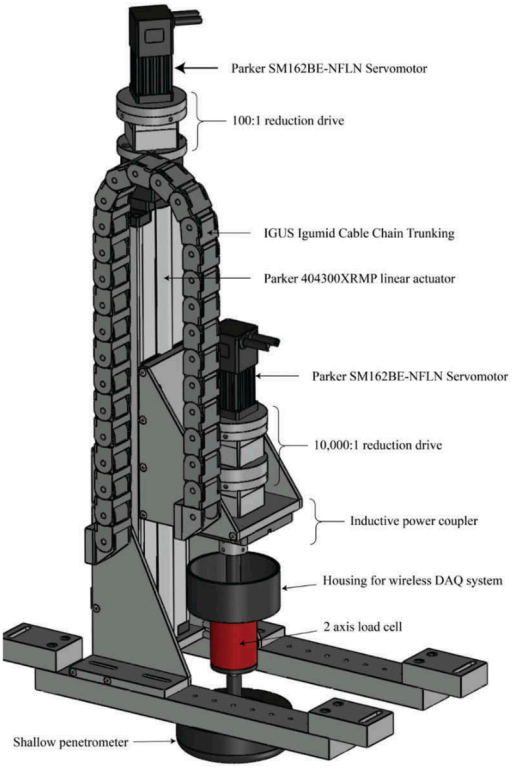

Figure 1. Penetrometer system: vertical and rotational actuation.

Figure 2. Miniature penetrometers: Ø5 × 20 mm T-bar, Ø10 mm ball, and Ø5 mm cone (MSMT Solutions).

The shallow penetrometer actuator system is capable of operation offshore on deck, in box cores. However, it is equally suited to use in the laboratory, with recovered samples. Both modes have been used.

2.2 *Miniature vertical penetrometers*

To measure the shallow strength profiles of samples, miniature scaled versions of the conventional cone, ball and T-bar penetrometers are used. These attach via simple fittings to the same actuator, and provide high resolution profiles of shear strength. For the ball and T-bar, remoulded strength is also obtained through a cyclic phase. The penetrometers shown in Figure 2 have replaceable top load cells and were manufactured by MSMT Solutions (Perth, Australia).

2.3 *Shallow rotational penetrometers*

Three shallow rotational penetrometers are shown in Figure 3: ring and toroid penetrometers of outer diameter, D_o = 125 mm, and body width or diameter, D_b = 25 mm, and a hemiball with overall diameter, D = 100 mm. All penetrometers are roughened by a sand coating and feature embedded pore pressure transducers with porous stones flush with the curved surfaces.

2.4 *Sampling and testing location*

The penetrometer system mounts onto box cores, or can rest on a frame over a sample. Tests on intact samples can be performed in box cores on deck, or jumbo samples can be extracted from a box core (e.g. in a 250 mm diameter plastic tube) and transported back to the lab for penetrometer testing (Figure 4).

A typical combined testing programme for a single box or jumbo core involves (i) vertical penetrometer tests to assess the strength profile, followed by (ii) one or more shallow penetrometer tests to measure interface strength and near-surface consolidation

Figure 3. Shallow penetrometers: ring, toroid and hemiball.

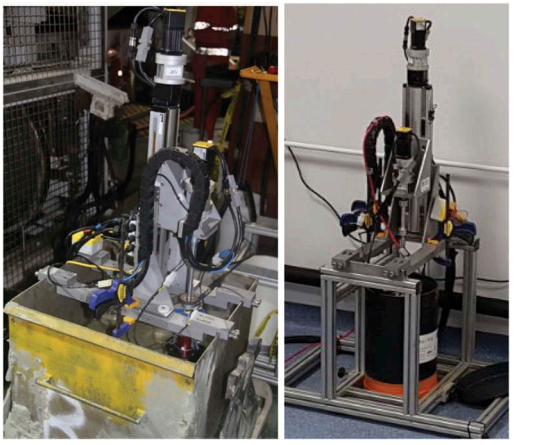

Figure 4. Testing on deck (left) and in the lab (right).

properties. If insufficient surface area is available, extra shallow penetrometer tests can be performed after scraping away the top layer or on remoulded samples.

3 STRENGTH PROFILING

Example profiles from the miniature vertical penetrometers are shown in Figure 5, for conditions with penetration resistance from 10 to 1000 kPa.

T-bar tests in very soft clay (Figure 5a) resolve the undrained strength, s_u, to 1/10th of a kPa, and are consistent with shallow penetrometer strength data. Miniature cone and T-bar data from undrained penetration in carbonate silt (Figure 5b) show consistent penetration resistance across both instruments, and agreement with standard (D = 35.7 mm) cone data from a seabed frame system. However, for the sandy silt example (Figure 5c), the initial penetration resistance of the standard cone is lower, perhaps due to near-surface effects on the penetration mechanism, which have minimal influence on the miniature cone.

4 SHALLOW PENETROMETER TESTING

4.1 *Typical test procedure*

The usual steps of a shallow penetrometer test are illustrated in Figure 6. The steps are described in Table 1, which sets out the control applied to the vertical and rotational axes in each step, the end points of each step and the typical speed or durations

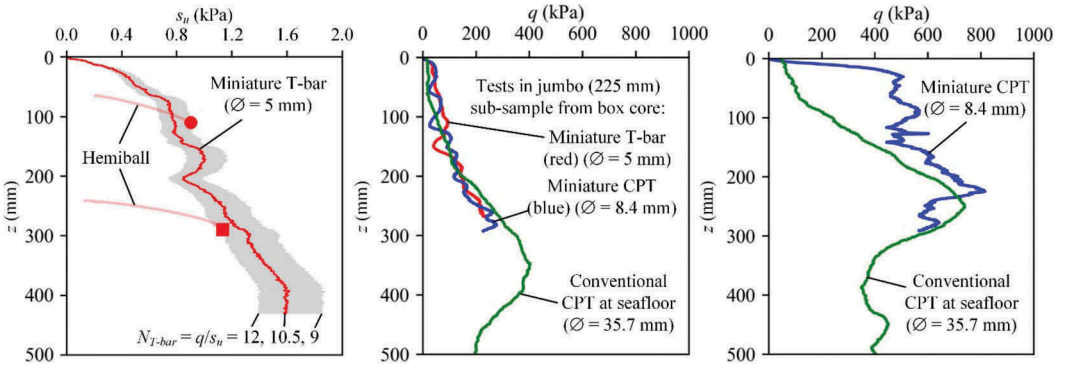

Figure 5. Vertical penetrometer tests in intact seabed samples (i) Clay (ii) Carbonate silt (iii) Carbonate sandy silt.

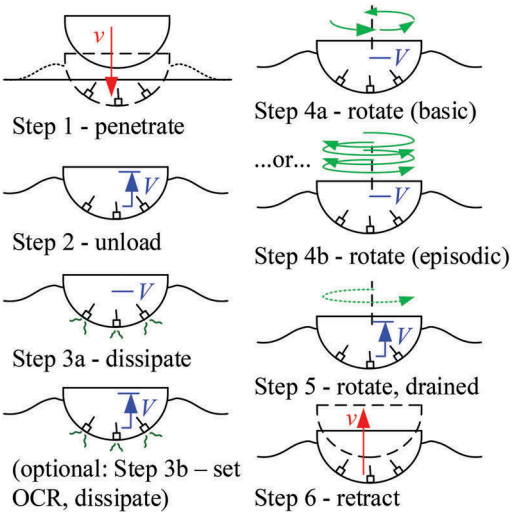

Figure 6. Stages of a shallow rotational penetrometer test.

relevant to testing in soft clay. On sandy soils the periods are more rapid, and the dissipation pauses may not be required. Figure 7 shows typical raw results.

4.2 *Typical test results*

The usual interpretation procedure for a shallow penetrometer test is set out in Table 2, and the interpreted data is shown in Figure 8. The interpretation methods for soil strength and consolidation parameters are based on bearing capacity theory and dissipation solutions. The interface strength parameters derived from the rotational stages involve a correction for 'wedging' effects for the hemiball and toroid devices. Ring penetrometer data does not need this correction.

Ideally, fully undrained and fully drained strengths can be measured, limited by the maximum actuator speed and test duration, respectively, relative to the soil coefficient of consolidation. Regard-

Table 1. Typical shallow penetrometer test procedure.

Step	Step name	Control parameters	Control values (toroid and ring)	Step procedure	Step end point
0	Prepare	Vertical rate, v Rotation rate, $\omega = 0$	$v = 0.5$ mm/s	Position penetrometer above test location in sample and drive penetrometer to test start point. Take zero readings from all transducers. Confirm response of pore pressure transducers to hydrostatic head.	Visual check: penetrometer is ~20 mm above sample surface
1	Penetrate	Vertical rate, v Rotation rate, $\omega = 0$	$v = 0.4$ mm/s	Drive penetrometer vertically to $0.5D$ embedment (or until the load cell limit, V_{limit}, is reached). Maximum measured vertical load is captured as V_{max}, and used in control of Step 2.	When $w = 0.5D$ or vertical load, $V = V_{limit}$
2	Unload	Vertical load, V Rotation rate, $\omega = 0$	$V = V_{max}/2$	Reduce vertical load on penetrometer by a factor of 2, to $V = V_{max}/2$, (to avoid excessive settlement during rotational stage of test) and hold this load. (Or unload to a specified V to match the applied stress relevant for design).	Move immediately to Step 3
3	Dissipate	Vertical load, V Rotation rate, $\omega = 0$	$V = V_{max}/2$	Hold penetrometer under load of $V = V_{max}/2$, allowing dissipation of excess pore pressure, Δu.	When $\Delta u/\Delta u_{ini} < 0.1$
3b	Set OCR, dissipate	Vertical load, V Rotation rate, $\omega = 0$	$V = (V_{max}/2)/OCR$	(Optional, *OCR test option*) Reduce vertical load by a specified ratio; repeat pore pressure dissipation. (Consider the OCR range relevant to design when planning tests. If needed, add Step 3b in some tests).	When $\Delta u/\Delta u_{ini} < 0.1$

(*Continued*)

Table 1. (Cont.)

4 (4a *or* 4b)	4a Twitch rotation	Vertical load, V Rotation rate, ω	Fast-medium-slow, $\Delta\theta$ = 20 deg rotation at each speed, ω = 0.4, 0.04, 0.004 deg/s	*Basic monotonic test option:* Rotate device by a specified angle, at fast, medium and then slow speeds, to measure the undrained (initially) and drained (later) torsional resistance, T.	When θ = 60°
	4b Episodic rotation	Vertical load, V Rotation rate, ω	ω = ±0.4 deg/s for $\Delta\theta$ = 20° t_{consol} = 30 min	*Episodic test option:* Perform episodes of rotation and consolidation. In each rotation stage turn through a fixed angle at the fast speed, alternating direction between cycles. During consolidation period, t_{consol}, between cycles, maintain vertical load. Typically the response stabilises after ~15 episodes.	When the cycles are complete
5	Drained sweep	Vertical load, V Rotation rate, ω	$dV/dt = -V_{max}/(2t_{unload})$ ω = 0.004 deg/s	Rotate penetrometer at constant slow speed while reducing the vertical load to zero over the unloading period, t_{unload}. Typically set t_{unload} ~ 30 minutes on clay. This step gives the change in T with V, measuring the friction across a range of normal stresses.	When V = 0 (i.e. when the penetrometer lifts away from the sample)
6	Retract	Vertical rate, v Rotation rate, ω = 0	v = –0.5 mm/s	Withdraw penetrometer vertically to above the sample surface. Take additional zero readings.	Penetrometer returns to starting position above sample surface

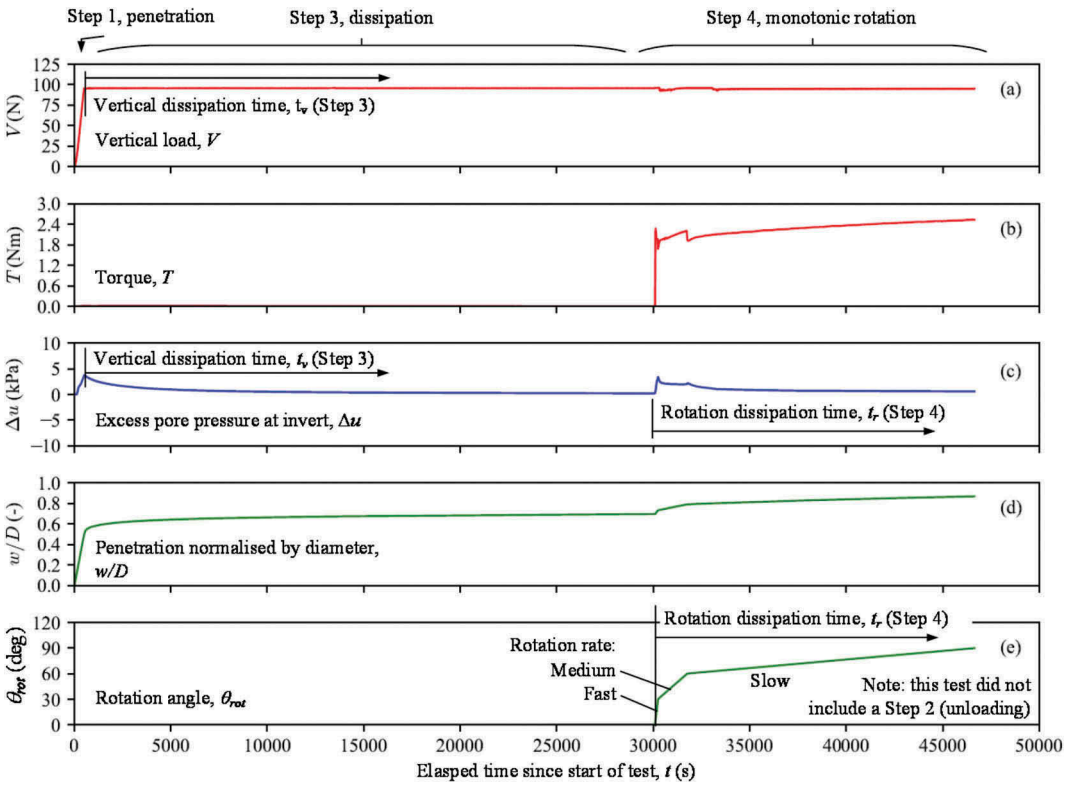

Figure 7. Typical unprocessed results from shallow penetrometer test with a monotonic rotation step (hemiball in soft clay).

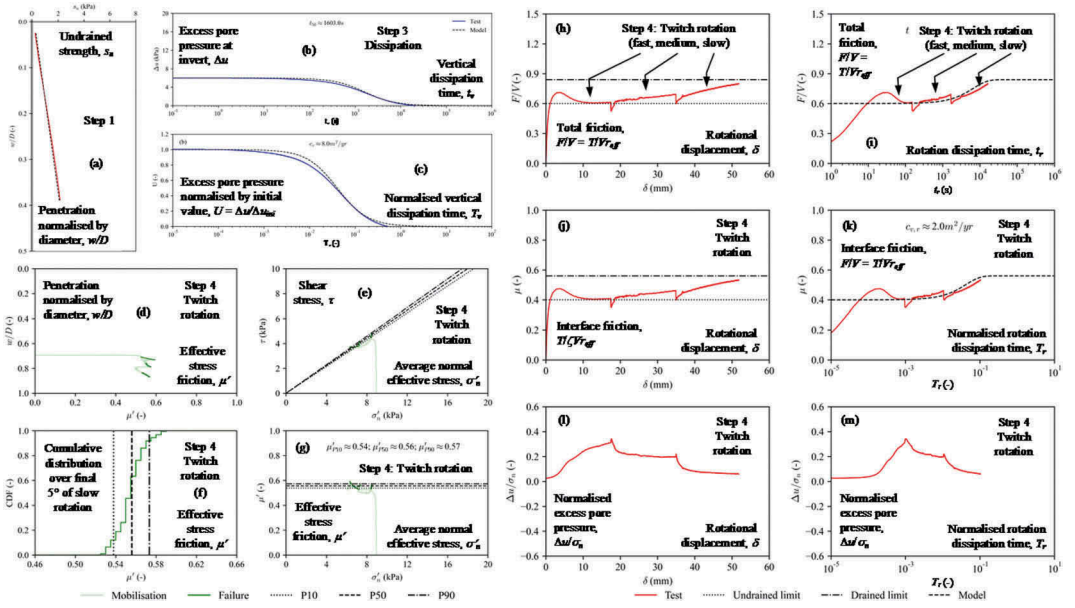

Figure 8. Typical interpreted results from a shallow penetrometer test with a monotonic rotation step (hemiball in soft clay).

less, an effective stress interpretation with a weighted average pore pressure provides effective friction parameters, even if the rotation is undrained or partially drained.

The interpreted results in Figure 8 show the following derived soil parameters: (i) profile of undrained strength, s_u (sub-figure (a)); (ii) consolidation coefficient during loading path (c); (iii) undrained interface strength (j); (iv) drained interface strength (j); (v) consolidation coefficient for shearing path (k); (vi) effective stress failure envelope (e) and (vii) effective stress friction (as distribution) (g).

5 RESEARCH STUDIES AND PROJECT USAGE

The penetrometer system has been used for >300 tests at the time of writing, for research activities and for commercial projects across three continents. Typical project test programmes have involved 10-20 shallow penetrometer tests spread over 3-4 distinct soil zones, with parallel vertical penetrometer profiling. Reliable and repeatable measurements of interface strength have been obtained for clays, silts and sands. Examples of added project value have included (i) the first ever data on consolidation coefficient at the very near-surface, (ii) better characterization of the consolidation-hardening behaviour from repeated surface sliding on clay and (iii) more detailed and repeatable measurements of drained and undrained interface strength parameters.

The shallow penetrometers offer an alternative to the low stress interface shear box. In our experience, this test can be unreliable compared to shallow penetrometer tests due to extraneous forces polluting the shear and normal forces measured in the shear box. Further studies into shallow penetrometers, particularly focusing on the ring, are reported by Mohr et al. 2022 and Singh et al. 2022.

6 CONCLUSIONS

Vertical and shallow rotational penetrometer tests together provide a new method to obtain a wider and more reliable set of near-surface seabed mechanical properties compared to conventional practice.

The equipment, procedures and interpretation approach for the new types of shallow penetrometer are now well-established, with the key details summarized in this paper. Drained and undrained interface strength parameters, as well as consolidation properties, can be objectively derived through rapid testing in box cores or samples recovered to the laboratory.

Table 2. Typical shallow penetrometer test interpretation procedure.

Step	Step name/ type	Input parameter(s)	Calculated parameter(s)	Calculation approach	Calculation coefficients	
					Ring	Toroid Hemiball
1	Penetration	Vertical load, V	Undrained shear strength, s_u	$s_{um}, k_{su} = f(V(w))$ – use iteration to fit a linear s_u profile ($s_u = s_{um} + k_{su}w$) (Stanier & White 2015) $U = \frac{\Delta u}{\Delta u_{ini}} = \frac{1}{1+\left(\frac{T_v}{T_{50,v}}\right)^m}$ with time $T_v = \frac{c_v t_v}{D^2}$	N/A	See S&W reference
3	Dissipation	Excess pore pressure response, $\Delta u(t_v)$	Consolidation coefficient, c_v (for stress path after vertical penetration)	Plot data and equation of $\Delta u/\Delta u_{ini}$ vs. t_v, adjust c_v. Or find $t_{v,50}$ when $\Delta u/\Delta u_{ini} = 0.5 \rightarrow c_v = T_{50,v}D^2/t_{v,50}$. t_v: time since start of dissipation (i.e. start of step 3).	$T_{50,v} = 0.0675$ $m = 1.00$ (Singh et al. 2022)	$T_{50,v}$ and m vary with w/D. See Schneider et al. (2020b)
			Undrained interface friction, μ_{ud} Drained interface friction, μ_{dr}	$\mu_{ud} = \frac{\tau_{int}}{\sigma'_n} = \frac{F}{V} = \left(\frac{T}{\zeta V r_{eff}}\right)_{ud}$ $\mu_{dr} = \mu'^{n0} = \tan\delta = \left(\frac{\tau_{int}}{\sigma'_n}\right)^n_{ud} = \frac{F}{V} = \left(\frac{T}{\zeta V r_{eff}}\right)_{dr}$	$\zeta = 1$ $r_{eff} = L + \frac{D_b^2}{12L}L = \frac{1}{2}(D_o - D_b)$	
4, 5	Rotation	Vertical load, V Torque, T Total friction, $\mu = T/V$ Excess pore pressure, $\Delta u(t_r)$	Consolidation coefficient, $c_{v,r}$ (for stress path during rotation)	$\mu = \mu_{dr} - (\mu_{dr} - \mu_{ud})0.5^{\left(\frac{T_r}{T_{50,r}}\right)}$ with $T_r = \frac{c_{v,r}t_r}{D^2}$ Use same method of fitting as described in Step 3. t_r: time since start of rotation (i.e. start of step 4).	$T_{50,r} = 0.25$ $n = 0.9$	ζ, r_{eff}, A_c and $\beta = \frac{\Delta u_{ave}}{\Delta u_{pos}}$ vary with w/D. See Schneider et al. (2020b, c)
			Effective stress envelope, μ'	$\mu' = \left(\frac{\tau_{int}}{\sigma'_{n,ave}}\right)$ where $\tau_{int} = \frac{T}{A_c}$ and $\sigma'_{n,ave} = \sigma_{n,ave} - \Delta u_{ave} = \frac{\zeta V}{A_c} - \beta \Delta u_{pos}$	$A_c = 2\pi D_b L$ $\beta = \frac{\Delta u_{ave}}{\Delta u_{pos}} \approx 0.7$ for pore pressure at mid radius	

These methods have been developed through >300 tests, supported by theoretical and numerical analysis, and have been applied in several commercial projects.

ACKNOWLEDGEMENTS

We acknowledge support from the RIGSS JIP (Fugro, Total, Woodside and Shell), the EPSRC Offshore Renewable Energy Supergen Hub (grant EP/S000747/1) and Prof. Mark Randolph and Dr Mark Schneider.

REFERENCES

Boscardin, A.G. & DeGroot, D.J. 2015. Evaluation of a toroid for model pipeline testing of very soft offshore box core samples. Proc. ISFOG2015, Taylor & Francis, London: 363–368.

ISO 19901-4:2022. Specific requirements for offshore structures — Part 4: Geotechnical design considerations. ISO (draft).

Mohr H., Stanier S.A. & White D.J. 2022. The ring penetrometer for interface shear testing on sand. Geotechnique. In review.

Schneider M., Stanier S., White D.J. & Randolph M.F. 2020a. Apparatus for measuring pipe-soil interaction behaviour using shallow 'pipe-like' penetrometers. ASTM Geotechnical Testing Journal 43(3): 622–640.

Schneider M., Stanier S., White D.J. & Randolph M.F. 2020b. Shallow penetrometer tests: theoretical and experimental modelling of the penetration and dissipation stages. Canadian Geotechnical Journal 57(4): 568–579

Schneider M., Stanier S., White D.J. & Randolph M.F. 2020c. Shallow penetrometer tests: theoretical and experimental modelling of the rotation stage. Can. Geot. J. 57(4):568–579

Singh V., Mohr H., Stanier S.A. Bienen B. & Randolph M. F. 2022. Characterisation of interface friction strain-rate dependency of soft sediments at low stresses using a ring penetrometer. Geotechnique. In review.

Stanier, S. & White D.J. 2015. Shallow penetrometer penetration resistance. ASCE J. Geo Geoenv. Eng. 141 (3):04014117

White D.J., Stanier S.A., Schneider M., O'Loughlin C.D., Chow S.H., Randolph M.F., Draper S.D., Mohr H., Morton J.P., Peuchen, J., Chow F.C., Fearon R. & Roux A. 2017. Remote intelligent geotechnical seabed surveys – technology emerging from the RIGSS JIP. Proc. Int. Conf. OSIG. 1214–1222

White, D.J, Clukey EC, Randolph MF, Boylan NP, Bransby MF, Zakeri A, Hill AJ, Jaeck C. 2017. The state of knowledge of pipe-soil interaction for on-bottom pipeline design. OTC 27623, Proc. Offshore Technology Conference, Houston.

Yan Y., White D.J. & Randolph M.F. 2010. Investigations into novel shallow penetrometers for fine-grained soils. Proc. 2nd ISFOG. Perth. 321–326.

Yan Y., White D.J. & Randolph M.F. 2017. Elastoplastic consolidation solutions for scaling from shallow penetrometers to pipelines. Canadian Geotechnical Journal 54:881–895.